International Journal of Minerals, Metallurgy and Materials
Volume 30, Number 5, May 2023, Page 959
https://doi.org/10.1007/s12613-022-2542-0

Preparation and property of self-sealed plasma electrolytic oxide coating on magnesium alloy

Chen Ma, *Dong Wang*, *Jinyu Liu*, *Ning Peng*, *Wei Shang*✉, *and Yuqing Wen*✉

Guangxi Key Laboratory of Electrochemical and Magnetochemical Function Materials, College of Chemistry and Bioengineering, Guilin University of Technology, Guilin 541004, China

(Received: 17 May 2022; revised: 25 August 2022; accepted: 26 August 2022)

Abstract: Plasma electrochemical oxidation (PEO) is a surface modification technology to form ceramic coatings on magnesium alloys. However, its application is limited due to its defects. This work reports a novel preparation of *in-situ* sealing of PEO coatings by four-layer voltage and sol addition. The morphology and structure were characterized by scanning electron microscopy (SEM), energy dispersive X-ray spectroscopy (EDS), and X-ray diffractometer (XRD). Image-Pro Plus 6.0 was used to determine the porosity of the coating, which was decreased from 8.53% to 0.51%. Simultaneously, the coating thickness was increased by a factor of four. The anti-corrosion performance of each sample was evaluated using electrochemical tests, and the findings revealed that the corrosion current density of coatings (i_{corr}) of the samples were lowered from 9.152×10^{-2} to 6.152×10^{-4} mA·cm^{-2}, and the total resistance (R_T) of the samples were enhanced from 2.19×10^4 to 2.33×10^5 Ω·cm^2. The salt spray test used to simulate the actual environment showed that corrosion points appeared on the surface of the coating only at the 336 h. In addition, the mechanism of PEO self-sealing behavior was described in this article.

Keywords: magnesium alloy; *in-situ* sealing; plasma electrolytic oxidation; corrosion resistance

1. Introduction

The reserve of magnesium ranks eighth in the world [1], and it is one of the most abundant light metal elements [2–3]. Due to the unique features [4], it has been applied in various modern engineering fields in recent years [5]. However, the standard electrode potential of magnesium alloy is extremely negative, and it is easily corroded by corrosive media [6]. Therefore, in order to increase the application space of magnesium alloys, it is imperative to improve its corrosion resistance [7]. At present, surface treatment technology is considered to be the effective approach to reduce the corrosion rate of magnesium alloys at home and abroad, such as chemical conversion coating [8], anodizing [9–10], self-assembly [11–12], and sol–gel coating [13–14].

Among these surface treatment methods, plasma electrolytic oxidation (PEO) is a type of surface modification technology that forms a ceramic coating on the surface of magnesium alloys [15]. The limitation of the traditional anodizing voltage is broken by the PEO technology, which can form a uniform coating on the surface of various alloys [16]. PEO technology (also known as micro-arc oxidation technology) is a popular method due to its complete equipment, simple process, and good environmental friendliness [17–18]. The ceramic coating is grown *in-situ* in conjunction with the substrate, and the coating is tightly bonded to the substrate. In addition, PEO is an electrochemical and plasma chemical process [19], and it mainly uses the principle of dielectric breakdown [20]. When the voltage gradually increases, the sparks gradually become larger and the density increases, so micropores and microcracks are formed on the surface of the coating [21]. The substrate is corroded when the corrosive medium passes through the defects of the PEO coating. Hence, the corrosion resistance of the coating needs to be improved.

PEO process and the performance of the ceramic coating are affected by external and internal factors [22]. Intrinsic factors include the processing time of magnesium alloy pretreatment [23], the composition [24] and concentration [25] of the electrolyte. The external factors are composed of PEO electrical parameters [26], processing temperature [27], oxidation time [28], and additives [29]. Zou *et al*. [30] studied the effect of current frequency on the PEO coating. Their research showed that the corrosion current density decreases with the increasing of power supply current frequency, which means that the corrosion resistance is improved at higher current frequencies. Vakili-Azghandi *et al*. [26] reported that the PEO coatings formed without additives were denser and had lower corrosion rate when the current density decreased and the duty cycle and frequency were increased. However, changing the electrochemical parameters only reduces the porosity to a certain extent, and the micropores cannot be

✉ Corresponding authors: Wei Shang E-mail: 2001018@glut.edu.cn; Yuqing Wen E-mail: 2006027@glut.edu.cn

completely sealed. To overcome the shortcomings of the traditional PEO coating, it is necessary to improve the composition of the electrolyte solution and add additives to further realize the sealing. Cui *et al*. [31] have added K_2ZrF_6 to the micro-arc oxidation electrolyte. K_2ZrF_6 can provide coatings with two different melting point components, ZrO_2 (melting point 2680°C) and lower melting point MgF_2 (melting point 1890°C), which increases its corrosion resistance. Pak *et al*. [32] added organic solvents to the electrolyte to improve the corrosion resistance of coatings. Because the 3-aminopropyltrimethoxysilane (APTMS) and the long organic alkyl chain could form the Mg–O–Si chemical bond, the denser coating provides better corrosion resistance. Nadimi *et al*. [33] investigated the effect of adding ZrO_2 and ZnO nanoparticles and their composition on the PEO process coating. The results showed that ZnO and ZrO_2 nanoparticles have been deposited on the cavity and surface of the coating, and the corrosion resistance of the coating is significantly improved.

It is a long-standing quest in materials science to develop self-sealing coating based on a single material, without the need for oxidation and sealing. However, there are relatively few reports on the preparation method and corrosion resistance of magnesium alloy plasma electrolytic oxidation *in-situ* sealing so far. Therefore, this work reports that the PEO ceramic coating was prepared by four-layer of voltage, and the TiO_2 sol prepared in advance was added to the electrolyte for the first time. This method produces self-sealing PEO coatings with excellent corrosion resistance and extremely low porosity, without the need for subsequent sealing treatment. The findings will serve as a reference point for the future development of these self-sealing coatings.

2. Experimental

2.1. Materials

AZ91D magnesium alloy was used as the research object. Magnesium alloy samples (Al 8.5wt%, Zn 0.9wt%, Mn 0.3wt%, Si 0.13wt%, Cu 0.03wt%, and Mg Bal.) were cut into a size of 30 mm × 20 mm × 2 mm. At first, magnesium alloy substrates were polished with 600#, 800#, 1000#, and 1200# metallographic sandpaper in turn until the surfaces were smooth and flat. The dried samples were placed in an alkaline degreasing solution (20 $g\cdot L^{-1}$ NaOH, 30 $g\cdot L^{-1}$ Na_2CO_3, and 20 $g\cdot L^{-1}$ Na_3PO_4) at 70°C for 60 s to remove oil. Subsequently, the samples were cleaned in absolute ethanol and deionized water for 10 min by an ultrasonic cleaning machine. Finally, the cleaned samples were dried in a blast dryer at 50°C.

2.2. Preparation of coating

The pretreated magnesium alloy sample was immersed in a PEO solution (5 $g\cdot L^{-1}$ $Na_6P_6O_{18}$, 10 $g\cdot L^{-1}$ NaF, 10 $g\cdot L^{-1}$ KOH, 4 $g\cdot L^{-1}$ $Na_2B_4O_7$, 1 $g\cdot L^{-1}$ Na_2WO_4, 5 $mL\cdot L^{-1}$ $C_3H_8O_3$, 4 $mL\cdot L^{-1}$ $C_6H_{15}NO_3$, and 10 $g\cdot L^{-1}$ K_2ZrF_6) using a micro-arc oxidation power (JHMAO-380/20A, China) supply for plasma electrolytic oxidation. The constant parameters of the experiment were the frequency of 50 Hz, the duty cycle of 30.0%, and the given voltage of 30 V at the beginning of the experiment. The preparation method of the sol was as follows: 3 g TiO_2 was added to a beaker containing 100 mL of distilled water and stirred well. Then, the solution was irradiated with UV light for 2 h and broken up in an ultrasonic cleaner for 3 h.

Four different PEO coatings were prepared in this experiment. The PEO1 coating was the traditional PEO coating, whose voltage increased to 160 V at the frequency of 10 $V\cdot min^{-1}$ and then increased to 220 V at the frequency of 5 $V\cdot min^{-1}$. The PEO2 coating was based on PEO1 and the TiO_2 sol was continuously dropped during the experiment. The PEO3 is prepared by four-layer of voltage. The first-layer voltage was increased to 150 V at a frequency of 10 $V\cdot min^{-1}$ and then to 220 V at a frequency of 5 $V\cdot min^{-1}$. The secondary-layer voltage was first reduced by 40 V (220 to 180 V), raised to 220 V at a frequency of 10 $V\cdot min^{-1}$, and then increased to 240 V in the way of per increased by 5 V hold for 3 min. The voltage was finally raised to 280 V in this way, which was recorded as PEO3. The PEO4 coating was prepared by four-layer of voltage and adding TiO_2 sol. The time for adding TiO_2 was after the beginning of the secondary-layer of voltage. Fig. 1 shows the detailed preparation process of PEO coating.

2.3. Characterization

The surface, cross-sectional morphology and elemental composition of the PEO coatings were characterized by field emission scanning electron microscopy (FE-SEM, Japan) and energy dispersive X-ray spectroscopy (EDS, Germany). An X-ray diffractometer (XRD, Holland) with Cu K_α radiation (2θ: 5°–90°, λ = 0.154 nm) was used to characterize the surface structure of the PEO coatings. The thickness and roughness of each sample were measured by coating thickness gauge (TT260, China) and roughness tester (TR200, China). The surface of each sample at different positions was measured 5 times and averaged. The pore size, pore area, and porosity of every PEO coating were measured by Image-Pro Plus 6.0 software. The electrochemical impedance spectroscopy (EIS) and polarization curves of the PEO coatings of different samples were analyzed through the electrochemical workstation in 3.5wt% NaCl solution at room temperature. The traditional three-electrode system was used in this experiment. The saturated calomel electrode, the sample (effective test area of about 1 cm^2), and the platinum electrode was used as the reference electrode, the working electrode, and the auxiliary electrode, respectively. The EIS test of PEO coating was carried out under open circuit potential (OCP), and its frequency range and sinusoidal voltage amplitude were 10^5–10^{-2} Hz and 10 mV. The polarization curve test was obtained under the conditions of scanning range and scanning speed of (E_{OCP} ± 300) mV and 1 $mV\cdot s^{-1}$, respectively. The EIS and polarization curves of the coatings were processed by the ZView2 software and electrochemical workstation.

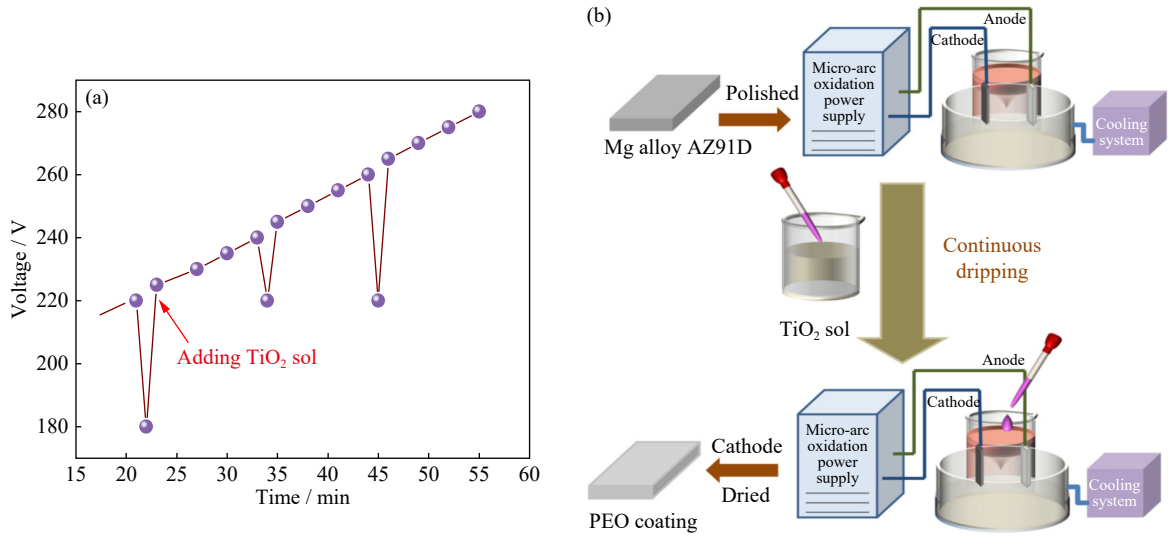

Fig. 1. PEO coating on the surface of magnesium alloy: (a) the four-layer voltage and time of adding TiO_2 sol; (b) preparation process.

The different PEO coatings were placed in a closed salt spray environment (AC-60B, China) containing 5.0wt% NaCl to evaluate the corrosion resistance.

3. Results and discussion

3.1. Characterization of different PEO coatings

Fig. 2 shows the surface microstructures of the four PEO coatings. Fig. 2(a1)–(a4) shows the traditional plasma electrolytic oxide coating (PEO1). As can be seen, there are large pore size and a large number of typical pit-like morphologies on the coating surface, which can be attributed to the continuously increased pressure to break down the coating during the process of forming the coating. Corrosive media can easily penetrate these holes to destroy the coating, so it cannot provide long-term protection for the substrate. Fig. 2(b1)–(b4) shows the PEO coating with sol added (PEO2). Compared with the traditional PEO coating, a certain amount

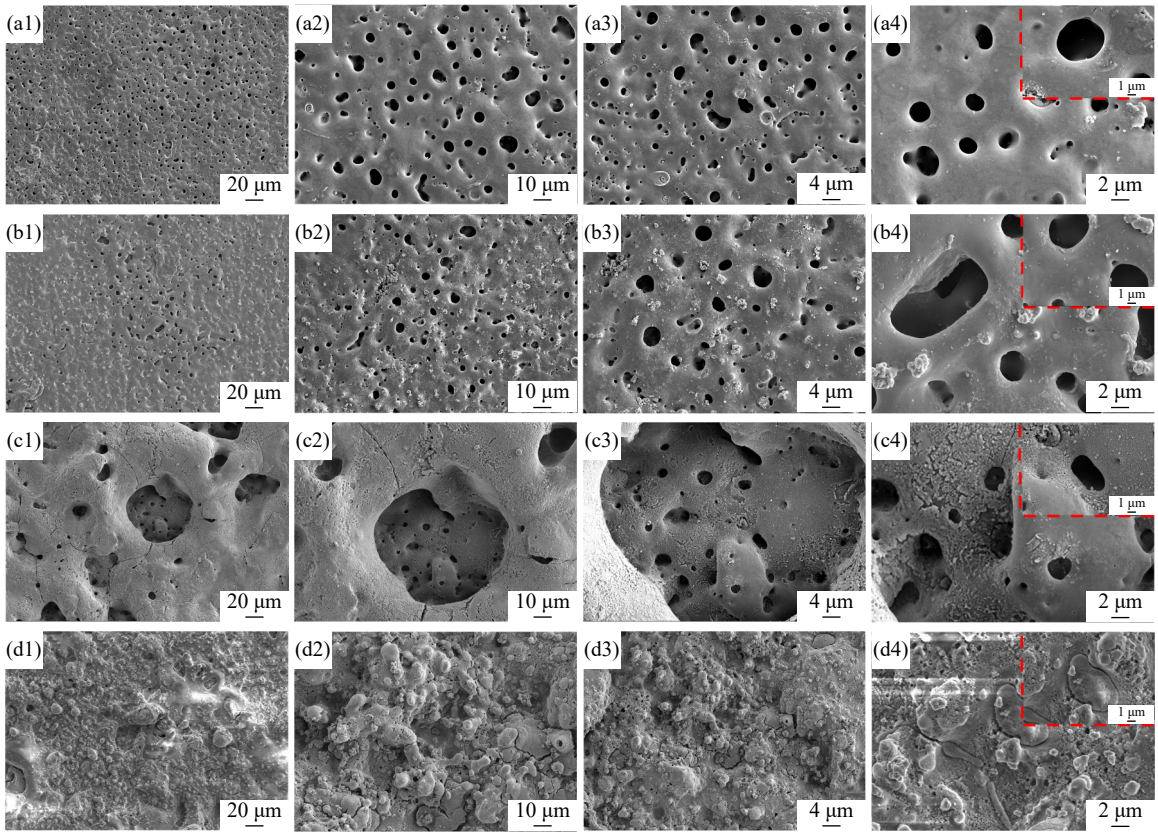

Fig. 2. SEM images of different coatings: (a1–a4) PEO1 coating; (b1–b4) PEO2 coating; (c1–c4) PEO3 coating; (d1–d4) PEO4 coating.

of particles are firmly adhered to the surface of the PEO coating. These particles are not uniformly distributed on the surface of the PEO coating and are distributed around the pores in the form of small debris. A small part of the pores is blocked by these particles, but a large number of larger pores are still exposed. Fig. 2(c1)–(c4) shows the PEO coating fabrication by four-layer of voltage (PEO3), the larger pore size is exposed, but the number of pores decreases, which is a kind of "hole sleeve hole" morphology. This may be because a new layer of PEO coating is formed on the surface of the existing PEO coating by using the method of boost-buck-boost again. Because the arc starting position is not fixed, the micro-holes cannot be completely sealed. Fig. 2(d1)–(d4) is the PEO coating formed by the *in-situ* method using four-layer of voltage and sol (PEO4). Molten particles are formed on the surface of the coating. The formed PEO coating is dense, uniform, and continuous, with almost no defects on the surface. Each micropore of the PEO coating has been completely sealed by these particles. Therefore, the protection of the substrate is greatly improved.

To confirm the elemental composition of different PEO coatings, Fig. 3 shows the elemental analysis of different coatings. According to the analysis of the EDS area, the contents of different elements in different PEO coatings are clearly shown in Table 1. The elements of each PEO coating are composed of Zr, O, F, Na, Mg, Al, W, P, and K (EDS spectrum shows that Au is a conductive element), and they are evenly distributed on the coating. Mg and Al are related to the AZ91D magnesium alloy matrix, and other elements are derived from the electrolyte solution, which indicates that the matrix and electrolyte elements participate in the formation of the coating. The Ti element is derived from the added sol. Among them, the diffraction peaks of Mg, F, and O are relatively strong. Similarly, the element content of Mg, F, and O is also the highest. This is because MgO and MgF_2 are the main components in the PEO coating. PEO2 and PEO4 are two different samples with sol added, but the peak intensity and element content of Ti in PEO4 are much higher than that of PEO2 from the comparison of diffraction peaks and elemental analysis.

In order to further confirm the composition of the magnesium alloy surface coating, the phase structure was characterized by XRD patterns. Fig. 4 shows the characteristic XRD peaks of the four different coatings. As can be seen, MgF_2, MgO, $Mg_3(PO_4)_2$, and ZrO_2 are all characterized on the XRD pattern for four different coatings. It is worth noting that all coatings demonstrate strong ZrO_2 diffraction peak, but the content of ZrO_2 is very small from the EDS analysis. This may be attributed to the strong crystallinity of ZrO_2. The main phases of the PEO3 coating and the PEO1 coating are the same. This shows that this pressure method has no effect on the phase composition of the PEO coating. Compared with the diffraction patterns of PEO2 and PEO4 coating, new phases, appear in PEO4 coating, while only the diffraction

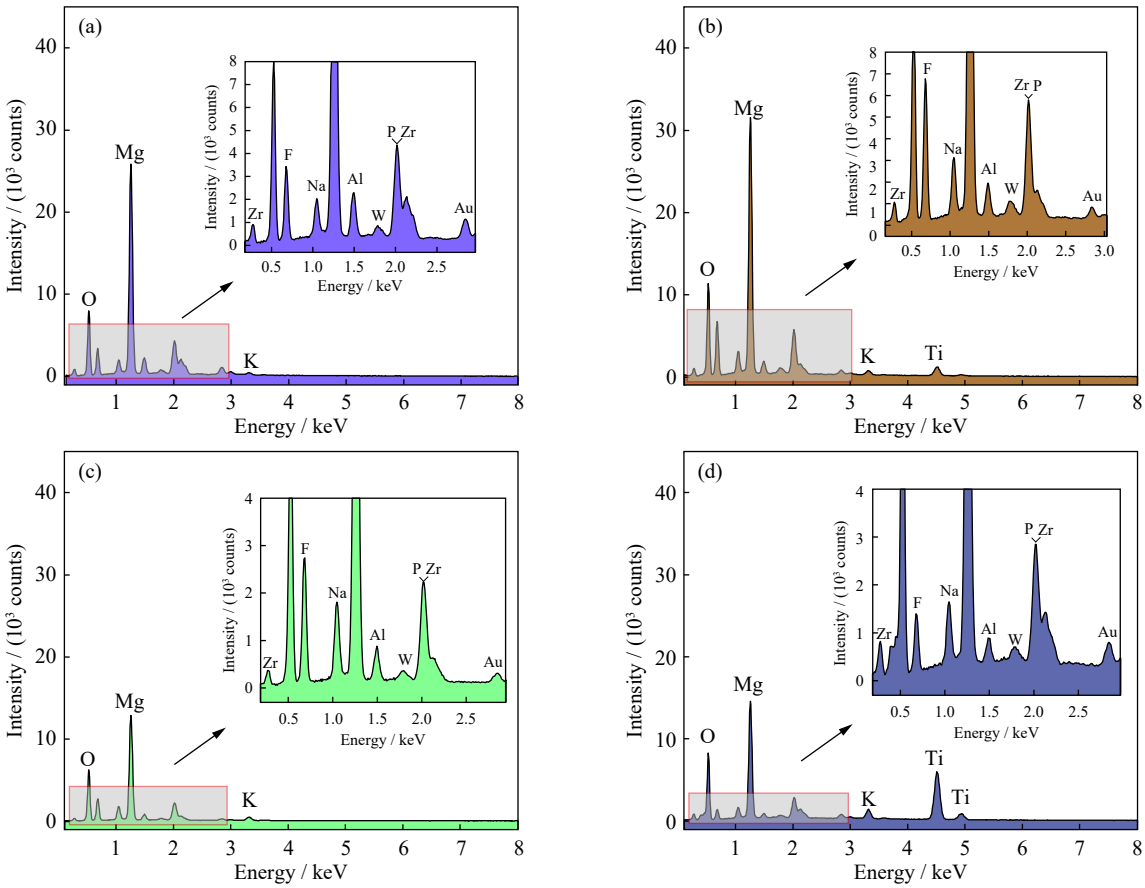

Fig. 3. EDS spectra of the surface of different PEO coatings: (a) PEO1 coating; (b) PEO2 coating; (c) PEO3 coating; (d) PEO4 coating.

Table 1. Main contents of different coating elements wt%

Coating	O	F	Mg	P	Zr	Ti
PEO1	22.23	9.32	27.45	5.70	3.54	—
PEO2	23.97	15.28	26.66	6.10	2.71	4.54
PEO3	22.28	11.33	33.38	4.52	2.10	—
PEO4	32.42	5.31	15.33	2.47	2.55	27.93

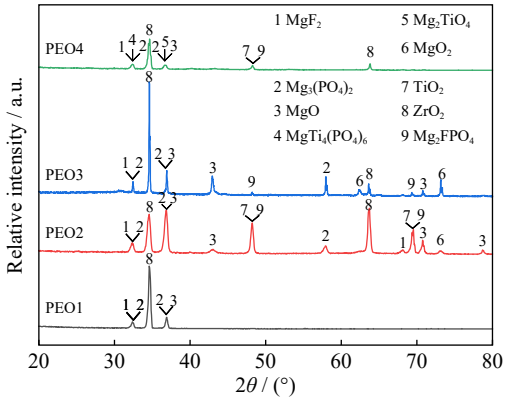

Fig. 4. XRD spectra of different PEO coatings.

peak of TiO_2 is found in PEO2. This is attributed to that TiO_2 is only adsorbed on the traditional PEO coating via preparation of PEO2, thus the sealing effect cannot be achieved. However, the PEO4 coating formed by using the quadruple voltage method and during the adding process TiO_2 is decomposed and chemically reacts with other ions, forming $MgTi_4(PO_4)_6$ and Mg_2TiO_4. Combined with the SEM image, there are not only attached particles on the coating, but also new phases will be formed and deposited on the surface of the coating. Using this method, a continuous and dense PEO coating is generated on the magnesium alloy substrate.

3.2. Cross-sectional morphology, thickness, and roughness of the PEO coatings

The cross-sectional morphology and element distribution of four different coatings can be clearly observed in Fig. 5. Large micropores and pores can be seen in Fig. 5(a)–(c). Although the porosity can be reduced by adding sol (Fig. 5(b)), only few TiO_2 particles are attached to the crosssection of the coating, and Ti element is hardly shown on the element distribution map. The coating formed by the four-layer of voltage method can clearly see that the increase in the thickness of the coating from Fig. 5(c), but the coating is not uniform and dense and has large pores. The corrosive medium easily penetrates the defects of the porous outer layer and the coating to corrode the substrate. The cross-sectional coating formed on the surface of the magnesium alloy by applying the sol and the four-layer of voltage is shown in Fig. 5(d). As can be seen in conjunction with Fig. 5(e), the entire coating is filled by the newly formed material instead of TiO_2 simply are attached to the surface of the coating. The new substance is generated on the coating and is firmly embedded in the PEO coating, which makes the layer have good continuity and adhesion and makes the coating surface uniform and dense.

The changes in the average thickness and roughness of the PEO coatings under different conditions are shown in Fig. 6. As can be seen, four-layer of voltage methods has no significant effect on the roughness of the PEO coating. The average roughness of the PEO1 coating is (0.506 ± 0.031) μm, slightly higher than PEO2 ((0.466 ± 0.029) μm) and lower than PEO3 ((0.529 ± 0.036) μm). Nevertheless, a combination of the adding TiO_2 sol and four-layer of voltage methods makes the roughness change a lot: the average roughness of the PEO4 coating is (0.402 ± 0.021) μm, which is consistent with the results reported by M. Krishtal *et al.* [34]. The reason for the decrease in surface roughness is that the presence of the sol reduces the plasma discharge energy, which reduces the average height between the hills and valleys on the coating surface. At the same time, the blockage and filling of the pores by the particles will also make it smooth.

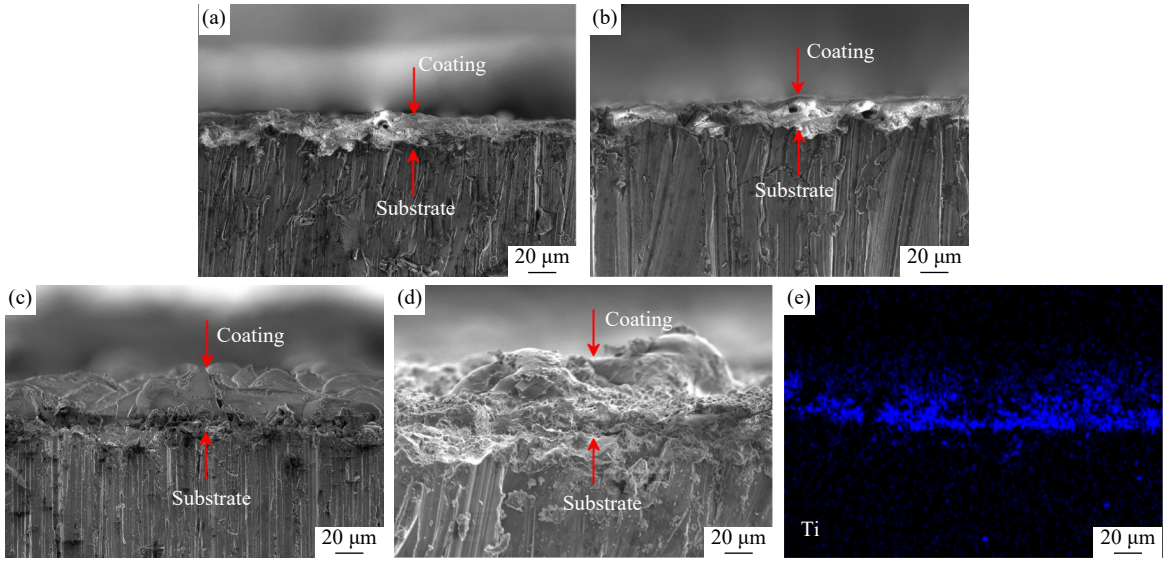

Fig. 5. Cross-sectional morphology of PEO coatings and EDS analysis: (a) PEO1; (b) PEO2; (c) PEO3; (d, e) PEO4 and Ti element distribution.

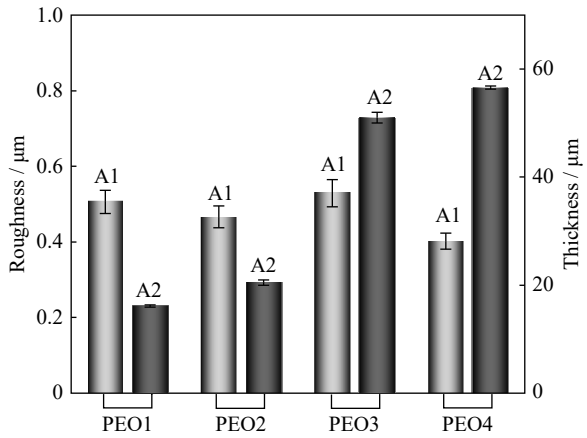

Fig. 6. Average surface roughness (A1) and thickness (A2) of different PEO coatings.

In addition, the thickness of different coatings demonstrates that the use of the four-layer of voltage of "boost-buck-boost again" gives the PEO coating a stage of "arcing-extinguishing- reburing arc", and the coating is continuously grown on the PEO coating. There is a factor of four increase in coating thickness compared to PEO1. This may be due to the pressing method will re-grow a coating on the original coating, which greatly increases the thickness of the coating. After adding TiO_2 sol, the average thickness of PEO coating increased from (16.12 ± 0.22) (PEO1) to (20.50 ± 0.50) μm (PEO2) and from (51.02 ± 0.98) (PEO3) to (56.58 ± 0.32) μm (PEO4), which is basically consistent with the cross-sectional micrographs. This may be due to the melting and solidification of TiO_2 particles on the surface coating during each discharge process, resulting in a certain increase in the coating thickness. This indicates that the presence of TiO_2 in the electrolyte will cause the thickness of the PEO coating to change, which is consistent with the results reported by Li *et al*. [35].

3.3. Pore diameter, pore area, and porosity of different PEO coatings

Fig. 7 summarizes the pore size, pore area, and porosity of different PEO coatings. The results show that the relative porosity of PEO1, PEO2, PEO3, and PEO4 coatings are 8.43%, 7.22%, 5.81%, and 0.51%, respectively. This is because of the presence of TiO_2 in the electrolyte reduces the plasma discharge energy density and the generation of new substances blocks the micropores on the surface of the PEO coating, resulting in a decrease in the relative porosity. Nearly three-quarters of the micropores on the PEO1, PEO2, and PEO3 coatings have pore diameters in the range of 0.75–2.75 μm, and the pore area in the range of 0.5–4.5 μm^2. The remaining pore diameters are in the range of 2.75–3.75 μm and the pore area is in the range of 4.5–7.5 μm^2. However, the pore diameters of the PEO4 coating micropores are almost all in the range of 0–0.1 μm, and the pore area is in the range of 0.0020–0.0025 μm^2. Generally, the measured value of the pore diameter of the micropore is below 0.1 μm, and the measured value of the pore area is within the range of 0.0020–0.0025 μm^2, which cannot be counted as micropores. Therefore, the *in-situ* sealing method designed in this work make the coating completely closed.

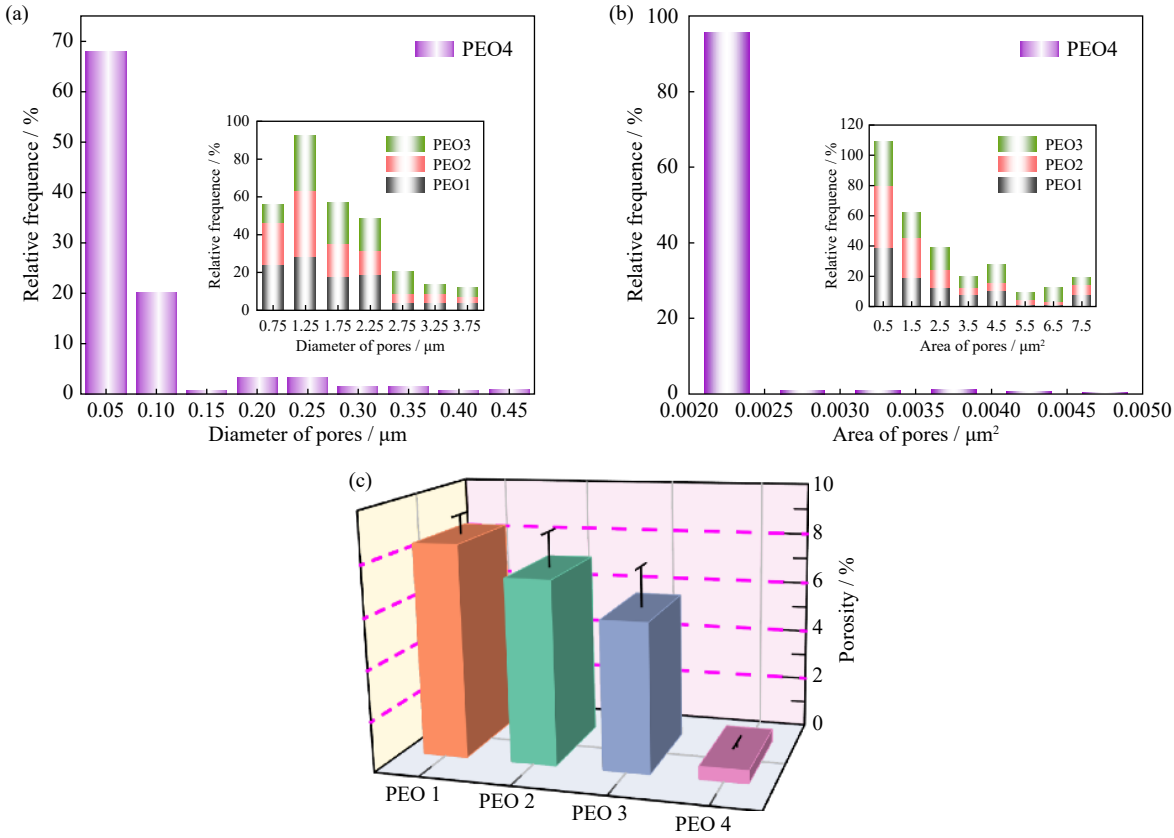

Fig. 7. Parameters of different PEO coatings: (a) pore diameter; (b) pore area; (c) porosity.

3.4. Anti-corrosion performance

Fig. 8 shows the potentiodynamic polarization curves and corrosion inhibition efficiency (η_P) and corrosion rate (C_R) of PEO1, PEO2, PEO3, and PEO4 coatings. The η_P of different coatings is calculated according to the formula Eq. (1) and C_R is calculated according to the formula Eq. (2) [36]. At the same time, the results of Tafel fitting data are shown in Table 2.

$$\eta_P = \frac{i^0_{corr} - i_{corr}}{i^0_{corr}} \times 100\% \quad (1)$$

$$C_R = 22.85 \times i_{corr} \quad (2)$$

where i^0_{corr} and i_{corr} are corrosion current density of magnesium alloy substrates and coatings, respectively, mA·cm^{-2}.

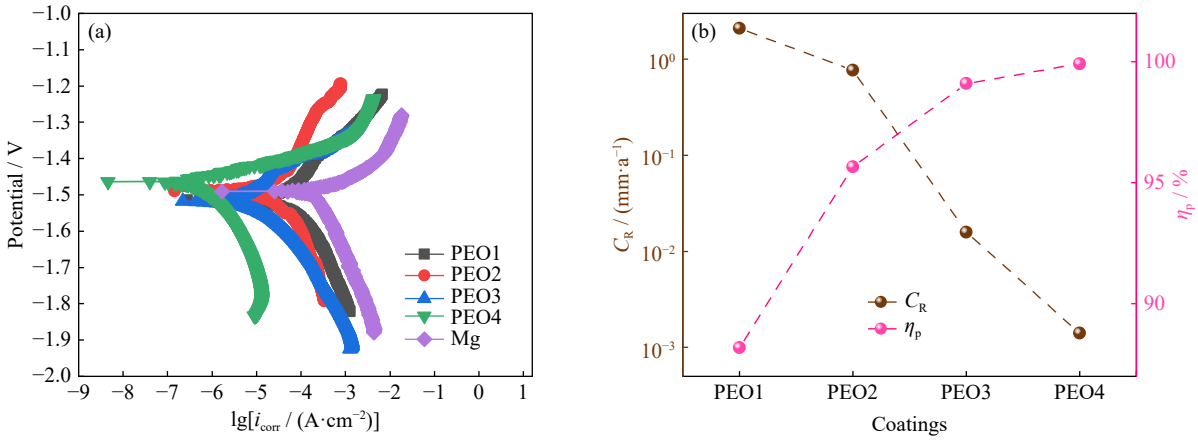

Fig. 8. (a) Potentiodynamic polarization curves of PEO coatings in 3.5wt% NaCl solution and (b) C_R and η_p of different samples.

Table 2. Polarization curve fitting results of different PEO coatings

Sample	E_{corr} / mV	β_a / (mV·dec^{-1})	β_c / (mV·dec^{-1})	i_{corr} / (mA·cm^{-2})	C_R / (mm·a^{-1})	η_p / %
Mg	−1490	4.259	8.609	7.750×10^{-1}	17.709	—
PEO1	−1514	5.261	5.855	9.152×10^{-2}	2.091	88.19
PEO2	−1489	4.393	5.448	3.373×10^{-2}	7.707×10^{-1}	95.65
PEO3	−1581	12.712	7.971	6.922×10^{-3}	1.582×10^{-2}	99.10
PEO4	−1463	25.265	5.967	6.152×10^{-4}	1.406×10^{-3}	99.92

From the perspective of kinetic analysis, the instantaneous corrosion rate of different coatings is evaluated using i_{corr} measurements. The lower the i_{corr} and C_R is, the better the corrosion resistance is [37]. From a thermodynamic point of view, E_{corr} is not used to evaluate the corrosion resistance of the coating [38]. Simultaneously, the corrosion resistance of the coating is judged by the η_p. The i_{corr} and C_R of the PEO1 are 7.750×10^{-1} mA·cm^{-2} and 2.091×10^{-3} mm·a^{-1}, respectively. This coating has a great tendency to corrode. The i_{corr} value of PEO2, PEO3, and PEO4 decreases successively, and the corrosion resistance gradually improves. As the coating is free of pores and the coating becomes much uniform and dense, the i_{corr} value of PEO4 has a two-order decrease compared with PEO1. Considering the practical application significance, C_R and η_p are also the important indicator for evaluating coatings. The change of corrosion rate is proportional to i_{corr}, and PEO1 coating has the fastest corrosion rate with an η_p of only 88.19%. With the continuous improvement of the defects of the PEO coating, the corrosion rate of PEO coating has decreased by orders of magnitude, and the corrosion rate of the PEO4 coating reached the minimum value, which was only 1.406×10^{-3} mm·a^{-1}. Meanwhile, the η_p of PEO4 coating reached 99.92%, which demonstrate the excellent anti-corrosion properties of the self-sealing coating. From the data of i_{corr}, C_R, and η_p, it can be observed that as the micropores of the PEO coating are gradually sealed, the corrosive medium is difficult to penetrate the coating to further corrode the magnesium alloy, resulting in the excellent corrosion resistance coating.

In order to further study the corrosion resistance of different coatings, the EIS test was carried out in 3.5wt% NaCl solution. Fig. 9 summarizes the Nyquist plot test results and fitting results of different PEO coatings. Two capacitive arcs are clearly present in the PEO4 coating. Capacitive arcing at the high frequency region was owing to a charge transfer process due to electric double layer capacitance, and the capacitive loop at the intermediate frequency region was attributed to the coating resistance [39]. Generally, the corrosion resistance of the coating can be compared in the EIS spectrum: the larger the arc radius of the capacitive reactance is, the better the corrosion resistance of the coating is [40]. The capacitive arc resistance of PEO4 coating is much larger than that of other PEO coatings. This result shows that the designed new self-sealing coating (PEO4) has a good corrosion resistance effect. In order to better analyze the impedance spectra of the different PEO coatings and more accurately understand the corrosion process, the equivalent circuit is installed on the corresponding coating in Fig. 10. R_s represents the solution

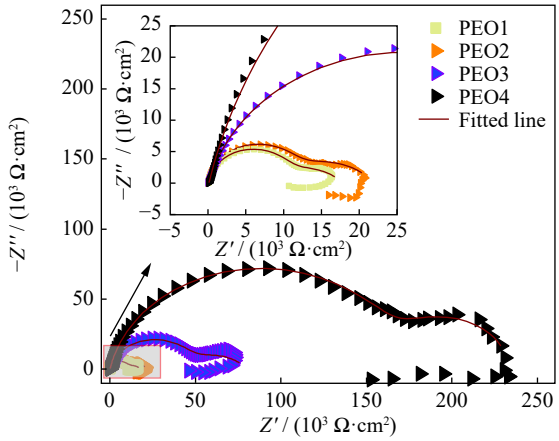

Fig. 9. EIS plots of the samples with different PEO coatings.

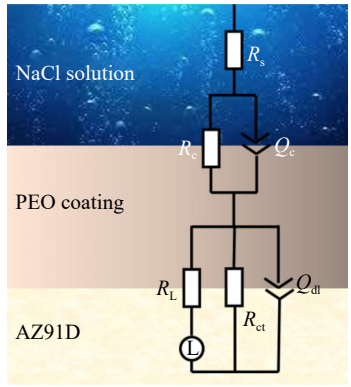

Fig. 10. Equivalent electric circuits for different PEO coating.

resistance, R_c and Q_c represent the coating resistance and capacitance corresponding to the surface coating effect, respectively, Q_{dl} represents the electric double layer capacitance of the reaction, and R_{ct} is the charge transfer resistance [41]. All capacitors are represented by constant-phase components, and the fitting results are shown in Table 3. The impedance of the CPE was computed by Eq. (3) [42].

$$Z_{CPE} = \frac{1}{Y_0 j\omega^n} \tag{3}$$

where Y_0 is the proportional factor, $j = \sqrt{-1}$, represents a vertical vector per unit length, ω represents the angular frequency, and the value of n ranges from 0.5 to 1.

Table 3. Fitted results of EIS plots of different PEO coatings

Sample	R_s / ($\Omega\cdot cm^2$)	Q_c / (10^{-7} F·cm^{-2})	n_1	R_c / (10^4 $\Omega\cdot cm^2$)	Q_{dl} / (10^{-5} F·cm^{-2})	n_2	R_{ct} / (10^4 $\Omega\cdot cm^2$)	R_T / (10^4 $\Omega\cdot cm^2$)
PEO1	11	8.90	0.96	0.98	4.49	0.59	0.79	1.77
PEO2	12	6.53	0.99	1.05	4.13	0.61	1.14	2.19
PEO3	14	2.17	0.87	4.62	1.67	0.59	3.36	7.98
PEO4	123	1.24	0.87	17.0	0.76	0.96	6.29	23.3

The total resistance R_T of the equivalent circuit is calculated by Eq. (4) [43].

$$R_T = R_c + R_{ct} \tag{4}$$

where R_c represents the coating resistance corresponding to the surface coating effect, R_{ct} is the charge transfer resistance, and R_T is the total resistance of the coating.

R_T is considered an significant parameter and plays an important role in evaluating the performance of the coating. Typically, the larger the value of R_T is [44], the better the anti-corrosion performance of the coating is. The R_T values of four PEO coatings were in the order of PEO4 > PEO3 > PEO2 > PEO1. The R_T value of PEO4 has reached the maximum value (2.33×10^5 $\Omega\cdot cm^2$), which has an order of magnitude improvement compared with the other three PEO coatings. Combining the electron microscope of four different PEO coatings, it can be seen that as the porosity of the PEO coating surface decreases, the self-sealing coating can be used as a physical barrier to more effectively inhibit the penetration of corrosive substances to the coating/substrate interface. In addition, because Mg_2TiO_4, TiO_2, and $MgTi_4(PO_4)_6$ occupies the channels (or pores), the density of the coating increases, enhancing the diffusion path of corrosion ions through the coating system, and further improving the corrosion resistance. Typically, the capacitance decreases as the porosity of the coating decreases. The fitting data shows that the PEO4 coating has a higher R_{ct} and a lower Q_{dl}, the defects of the PEO coating are constantly being improved, and the micropores are gradually sealed. According to the Nyquist diagram, the self-sealing PEO coating has good anti-corrosion properties for magnesium alloys.

In order to better explore the application of its coating performance in real life, four different samples were put into 5wt%NaCl environment for salt spray test. The neutral salt spray corrosion tests of different PEO coatings are shown in Fig. 11. The corrosion resistance of PEO1 and POE2 is extremely poor and corrosion points were observed on the surface of the coatings within 24 h. At the 168 h, partial corrosion is manifested in PEO2 coating, and the entire PEO1 coating was completely corroded. Compared with PEO1 and PEO2, the corrosion resistance of PEO3 is further improved. After 240 h of corrosion, pitting corrosion was gradually found on the edge of the PEO3 coating. After 336 h of corrosion, large-area corrosion was gradually discovered on the PEO3 coating. Compared with other coatings, the corrosion resistance of PEO4 coating has been further improved, and its anti-corrosion performance has reached the best, whose corrosion spots just appear on the edge of the PEO4 coating at 336 h.

3.5. Mechanism of the coating formation

The formation of the coating is affected by factors such as electrochemical parameters, metal surface conditions and

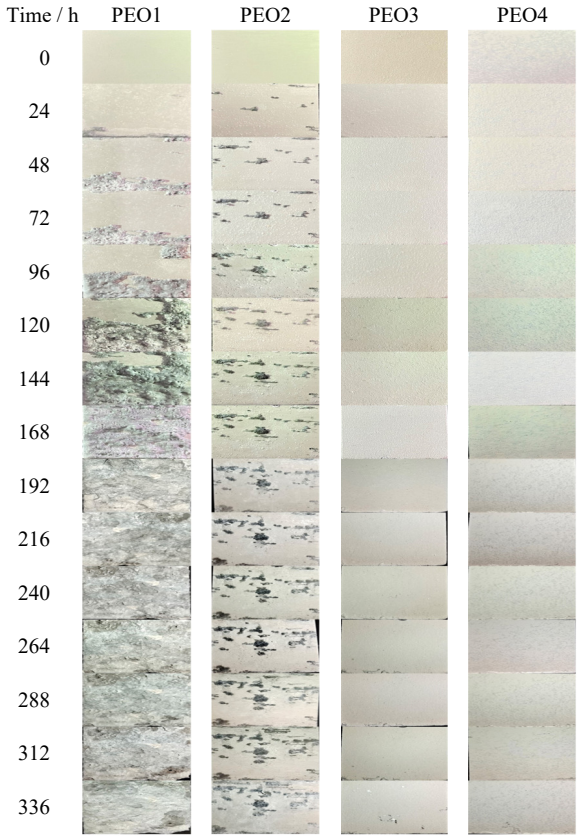

Fig. 11. Salt spray test of different samples.

electrolyte composition [43]. Based on the change of coating morphology and according to thermochemical, electrochemical and plasma reactions, the discussion on the formation mechanism of self-sealing coating is proposed. In addition, a schematic diagram of sealing the PEO coating by adding sol to four times of voltage is drawn, as shown in Fig. 12. When the oxidation process starts, the voltage is lower than the spark discharge voltage, and a thin passivation coating is formed on the magnesium alloy substrate [44]. There is no electric spark in this process, which is similar to the anodizing process [45]. As the voltage increases, the thickness of the coating also increases. When the voltage increases to the breakdown voltage, along with the electric spark phenomenon, there are more protrusions on the surface of the coating and its surface is also uneven. The number of protrusions on the oxide coating increases, and a large number are intertwined with each other, and a continuous porous structure of PEO coating is formed as shown in Fig. 12(a). Under the action of an electric field, Mg atoms lose electrons and become Mg ions. Simultaneously, some anions such as PO_4^{3-}, ZrF_6^{2-}, OH^-, and F^- will transfer to the surface of the substrate and deposit on the surface of the magnesium alloy to form a coating [34]. The stage of "arcing-extinguishing-reburing arc" is formed on the surface of the coating using a four-time voltage pressurization method, as shown in Fig. 12(b). Compared with the traditional PEO coating, the formation of a layer of coating on the existing coating makes the PEO coating much more continuous and dense, but still has pores. The main reactions were as follows:

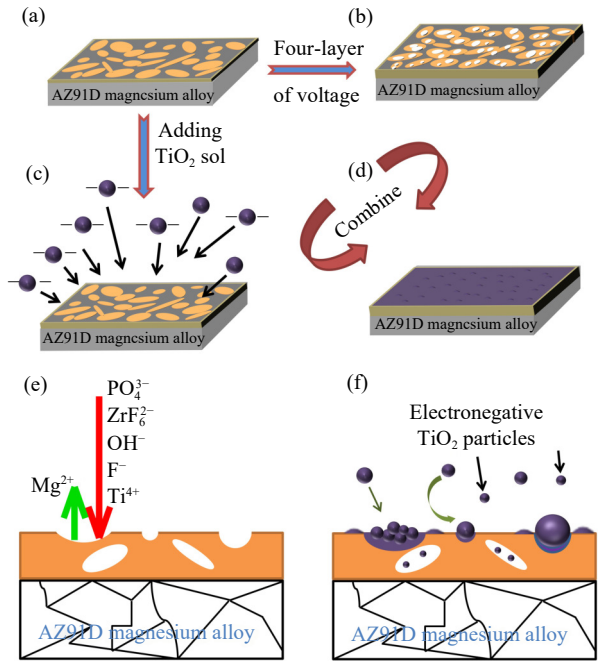

Fig. 12. Self-sealing coating formation mechanism: (a) PEO1 coating; (b) PEO3 coating; (c) negatively charged TiO_2 attracted to the PEO coating; (d) self-sealing coating (PEO4); (e) plasma discharge process; (f) side view of self-sealing coating.

$$Mg \rightarrow Mg^{2+} + 2e^- \quad (5)$$

$$2PO_4^{3-} + 3Mg^{2+} \rightarrow Mg_3(PO_4)_2 \quad (6)$$

$$2OH^- \rightarrow H_2O + O^{2-} \quad (7)$$

$$O^{2-} + Mg^{2+} \rightarrow MgO \quad (8)$$

$$ZrF_6^{2-} + 4OH^- \rightarrow ZrO_2 + 6F^- + 2H_2O \quad (9)$$

$$2F^- + Mg^{2+} \rightarrow MgF_2 \quad (10)$$

When the voltage is applied high enough, the sol is added to the electrolyte and becomes negatively charged after the electrolyte is distributed. With the continuous occurrence of electric sparks, channels are formed due to breakdown of the medium. Under the action of electrophoretic force, anions and negatively charged ions enter the charged channel and participate in the reaction, as shown in Fig. 12(c). Part of the TiO_2 particles are deposited in the discharge channel due to the eruption of the molten state oxidation during the microdischarge. As the voltage increases, the cooling rate difference between the inside and outside of the membrane increases, and these particles quickly solidify in contact with the electrolyte. In addition, TiO_2 has a lower melting point, and these particles solidify more slowly on the coating surface and deposit later. TiO_2 is adsorbed on the surface of the coating to block the micropores. Since the high temperature environment in the micro arc discharge area reaches 2000°C [46], Ti^{4+} and O^{2-} can be formed after TiO_2 is melted. This may be the reason for the formation of $MgTi_4(PO_4)_6$ and Mg_2TiO_4. The reaction is as follows:

$$TiO_2 \rightarrow Ti^{4+} + 2O^{2-} \quad (11)$$

$$Mg^{2+} + 4Ti^{4+} + 6PO_4^{3-} \rightarrow MgTi_4(PO_4)_6 \quad (12)$$

$$2Mg^{2+} + Ti^{4+} + 4O^{2-} \rightarrow Mg_2TiO_4 \quad (13)$$

Therefore, due to the blockage of micropores by particles and the formation of chemical substances on the surface of the coating, the self-sealing effect can be achieved well, as shown in Fig. 12(d). The cross-sectional schematic diagram of the self-sealing PEO coating formation process is shown in Fig. 12(e) and (f).

4. Conclusion

This work reports the *in-situ* sealing on PEO coatings by applying four-layer of voltage and adding TiO_2 sol. The surface of the prepared self-sealing coating is uniform and compact with almost no micropores, which is also proved by its appearance and relatively low porosity. New phases, $MgTi_4(PO_4)_6$ and Mg_2TiO_4, are grown on the surface of the coating compared to other coatings. The coating evaluation shows that the self-sealing coating had a factor of four increase in thickness, lower surface roughness, and better corrosion resistance. The difficulty of corrosive ions penetrating the coating is increased due to the presence of denser and thicker coatings. Compared with the traditional plasma electrolytic oxidation coating, the i_{corr} of the self-sealing coating has a reduction of two orders of magnitude. The C_R, η_p, and R_T of the self-sealing coating could reach 1.406×10^{-3} mm·a^{-1}, 99.92%, and 2.33×10^5 Ω·cm^2, respectively. Simultaneously, the salt spray test also confirms that the self-sealing coating can provide long-term stable protection for the substrate. Clogging of pores by particles and the formation of chemical substances on the surface of the coating are the keys to the formation of the self-sealing coating, demonstrating the significant influence of PEO coating microstructure on the protective performance of magnesium alloys.

Acknowledgements

This work was financially supported by the Guangxi Natural Science Foundation (No. 2020GXNSFAA159011) and the National Natural Science Foundation of China (No. 51664011).

Conflict of Interest

The authors declare no competing financial interest.

References

[1] Y. Yang, X.M. Xiong, J. Chen, X.D. Peng, D.L. Chen, and F.S. Pan, Research advances in magnesium and magnesium alloys worldwide in 2020, *J. Magnes. Alloys*, 9(2021), No. 3, p. 705.

[2] K. Luo, L. Zhang, G.H. Wu, W.C. Liu, and W.J. Ding, Effect of Y and Gd content on the microstructure and mechanical properties of Mg–Y–RE alloys, *J. Magnes. Alloys*, 7(2019), No. 2, p. 345.

[3] H.L. Huang and W.L. Yang, Corrosion behavior of AZ91D magnesium alloy in distilled water, *Arab. J. Chem.*, 13(2020), No. 7, p. 6044.

[4] G.Z. Kang and H. Li, Review on cyclic plasticity of magnesium alloys: Experiments and constitutive models, *Int. J. Miner. Metall. Mater.*, 28(2021), No. 4, p. 567.

[5] F. Samadpour, G. Faraji, and A. Siahsarani, Processing of AM60 magnesium alloy by hydrostatic cyclic expansion extrusion at elevated temperature as a new severe plastic deformation method, *Int. J. Miner. Metall. Mater.*, 27(2020), No. 5, p. 669.

[6] J.H. Chu, L.B. Tong, M. Wen, *et al*., Inhibited corrosion activity of biomimetic graphene-based coating on Mg alloy through a cerium intermediate layer, *Carbon*, 161(2020), p. 577.

[7] L.X. Li, Z.H. Xie, C. Fernandez, *et al*., Development of a thiophene derivative modified LDH coating for Mg alloy corrosion protection, *Electrochim. Acta*, 330(2020), art. No. 135186.

[8] G.Q. Duan, L.X. Yang, S.J. Liao, *et al*., Designing for the chemical conversion coating with high corrosion resistance and low electrical contact resistance on AZ91D magnesium alloy, *Corros. Sci.*, 135(2018), p. 197.

[9] Ö. Bayrak, H. Ghahramanzadeh Asl, and A. Ak, Protein adsorption, cell viability and corrosion properties of Ti_6Al_4V alloy treated by plasma oxidation and anodic oxidation, *Int. J. Miner. Metall. Mater.*, 27(2020), No. 9, p. 1269.

[10] Z.Q. Zhang, L. Wang, M.Q. Zeng, *et al*., Corrosion resistance and superhydrophobicity of one-step polypropylene coating on anodized AZ31 Mg alloy, *J. Magnes. Alloys*, 9(2021), No. 4, p. 1443.

[11] D. Jiang, H. Zhou, S. Wan, G.Y. Cai, and Z.H. Dong, Fabrication of superhydrophobic coating on magnesium alloy with improved corrosion resistance by combining micro-arc oxidation and cyclic assembly, *Surf. Coat. Technol.*, 339(2018), p. 155.

[12] Y.B. Zhao, L.Q. Shi, X.J. Ji, *et al*., Corrosion resistance and antibacterial properties of polysiloxane modified layer-by-layer assembled self-healing coating on magnesium alloy, *J. Colloid Interface Sci.*, 526(2018), p. 43.

[13] H. Ashassi-Sorkhabi, S. Moradi-Alavian, R. Jafari, A. Kazempour, and E. Asghari, Effect of amino acids and montmorillonite nanoparticles on improving the corrosion protection characteristics of hybrid sol–gel coating applied on AZ91 Mg alloy, *Mater. Chem. Phys.*, 225(2019), p. 298.

[14] T.X. Lu, C.G. Chen, Z.M. Guo, P. Li, and M.X. Guo, Tungsten nanoparticle-strengthened copper composite prepared by a sol-gel method and *in situ* reaction, *Int. J. Miner. Metall. Mater.*, 26(2019), No. 11, p. 1477.

[15] V. Dehnavi, W.J. Binns, J.J. Noël, D.W. Shoesmith, and B.L. Luan, Growth behaviour of low-energy plasma electrolytic oxidation coatings on a magnesium alloy, *J. Magnes. Alloys*, 6(2018), No. 3, p. 229.

[16] M. Roknian, A. Fattah-Alhosseini, S.O. Gashti, and M.K. Keshavarz, Study of the effect of ZnO nanoparticles addition to PEO coatings on pure titanium substrate: Microstructural analysis, antibacterial effect and corrosion behavior of coatings in Ringer's physiological solution, *J. Alloys Compd.*, 740(2018), p. 330.

[17] X.P. Lu, C. Blawert, K.U. Kainer, and M.L. Zheludkevich, Investigation of the formation mechanisms of plasma electrolytic oxidation coatings on Mg alloy AM50 using particles, *Electrochim. Acta*, 196(2016), p. 680.

[18] H. Tang and Y. Gao, Preparation and characterization of hydroxyapatite containing coating on AZ31 magnesium alloy by micro-arc oxidation, *J. Alloys Compd.*, 688(2016), p. 699.

[19] D.V. Mashtalyar, S.V. Gnedenkov, S.L. Sinebryukhov, I.M. Imshinetskiy, and A.V. Puz', Plasma electrolytic oxidation of the magnesium alloy MA8 in electrolytes containing TiN nanoparticles, *J. Mater. Sci. Technol.*, 33(2017), No. 5, p. 461.

[20] K.R. Wu, C.H. Hung, C.W. Yeh, and J.K. Wu, Microporous TiO_2–WO_3/TiO_2 films with visible-light photocatalytic activity synthesized by micro arc oxidation and DC magnetron sputtering, *Appl. Surf. Sci.*, 263(2012), p. 688.

[21] F. Muhaffel and H. Cimenoglu, Development of corrosion and wear resistant micro-arc oxidation coating on a magnesium alloy, *Surf. Coat. Technol.*, 357(2019), p. 822.
[22] A. Fattah-Alhosseini, K. Babaei, and M. Molaei, Plasma electrolytic oxidation (PEO) treatment of zinc and its alloys: A review, *Surf. Interfaces*, 18(2020), art. No. 100441.
[23] B.W. Zhu, L. Wang, Y.Z. Wu, W. Yue, J. Liang, and B.C. Cao, Improving corrosion resistance and biocompatibility of AZ31 magnesium alloy by ultrasonic cold forging and micro-arc oxidation, *J. Biomater. Appl.*, 36(2022), No. 9, p. 1664.
[24] M. Babaei, C. Dehghanian, P. Taheri, and M. Babaei, Effect of duty cycle and electrolyte additive on photocatalytic performance of TiO_2–ZrO_2 composite layers prepared on CP Ti by micro arc oxidation method, *Surf. Coat. Technol.*, 307(2016), p. 554.
[25] M. S. Joni and A. Fattah-Alhosseini, Effect of KOH concentration on the electrochemical behavior of coatings formed by pulsed DC micro-arc oxidation (MAO) on AZ31B Mg alloy, *J. Alloys Compd.*, 661(2016), p. 237.
[26] M. Vakili-Azghandi and A. Fattah-Alhosseini, Effects of duty cycle, current frequency, and current density on corrosion behavior of the plasma electrolytic oxidation coatings on 6061Al alloy in artificial seawater, *Metall. Mater. Trans. A*, 48(2017), No. 10, p. 4681.
[27] L.J. Bai, B.X. Dong, G.T. Chen, T. Xin, J.N. Wu, and X.D. Sun, Effect of positive pulse voltage on color value and corrosion property of magnesium alloy black micro-arc oxidation ceramic coating, *Surf. Coat. Technol.*, 374(2019), p. 402.
[28] Y.W. Song, K.H. Dong, D.Y. Shan, and E.H. Han, Investigation of a novel self-sealing pore micro-arc oxidation film on AM60 magnesium alloy, *J. Magnes. Alloys*, 1(2013), No. 1, p. 82.
[29] Z. Li, Z. Chen, S. Feng, T. Zhao, and W.Z. Wang, Effects of Na_2WO_4 on the MAO coatings on AZ80, *Surf. Eng.*, 36(2020), p. 817.
[30] B. Zou, G.H. Lü, G.L. Zhang, and Y.Y. Tian, Effect of current frequency on properties of coating formed by microarc oxidation on AZ91D magnesium alloy, *Trans. Nonferrous Met. Soc. China*, 25(2015), No. 5, p. 1500.
[31] X.J. Cui, C.H. Liu, R.S. Yang, M.T. Li, and X.Z. Lin, Self-sealing micro-arc oxidation coating on AZ91D Mg alloy and its formation mechanism, *Surf. Coat. Technol.*, 269(2015), p. 228.
[32] S.N. Pak, Z.P. Yao, K.S. Ju, C.N. Ri, and Q.X. Xia, Effect of organic additives on structure and corrosion resistance of MAO coating, *Vacuum*, 151(2018), p. 8.
[33] M. Nadimi and C. Dehghanian, Incorporation of ZnO–ZrO_2 nanoparticles into TiO_2 coatings obtained by PEO on Ti–6Al–4V substrate and evaluation of its corrosion behavior, microstructural and antibacterial effects exposed to SBF solution, *Ceram. Int.*, 47(2021), No. 23, p. 33413.
[34] M.M. Krishtal, P.V. Ivashin, I.S. Yasnikov, and A.V. Polunin, Effect of nanosize SiO_2 particles added into electrolyte on the composition and morphology of oxide layers formed in alloy AK6M2 under microarc oxidizing, *Met. Sci. Heat Treat.*, 57(2015), No. 7-8, p. 428.
[35] W.P. Li, M.Q. Tang, L.Q. Zhu, and H.C. Liu, Formation of microarc oxidation coatings on magnesium alloy with photocatalytic performance, *Appl. Surf. Sci.*, 258(2012), No. 24, p. 10017.
[36] Z.M. Shi, M. Liu, and A. Atrens, Measurement of the corrosion rate of magnesium alloys using Tafel extrapolation, *Corros. Sci.*, 52(2010), No. 2, p. 579.
[37] M.F. He, L. Liu, Y.T. Wu, Z.X. Tang, and W.B. Hu, Corrosion properties of surface-modified AZ91D magnesium alloy, *Corros. Sci.*, 50(2008), No. 12, p. 3267.
[38] T.F. Xiang, S.L. Zheng, M. Zhang, H.R. Sadig, and C. Li, Bioinspired slippery zinc phosphate coating for sustainable corrosion protection, *ACS Sustainable Chem. Eng.*, 6(2018), No. 8, p. 10960.
[39] M. Ramezanzadeh, B. Ramezanzadeh, M. Mahdavian, and G. Bahlakeh, Development of metal-organic framework (MOF) decorated graphene oxide nanoplatforms for anti-corrosion epoxy coatings, *Carbon*, 161(2020), p. 231.
[40] A.K. Behera, A. Das, S. Das, and A. Mallik, Electrochemically functionalized graphene as an anti-corrosion reinforcement in Cu matrix composite thin films, *Int. J. Miner. Metall. Mater.*, 28(2021), No. 9, p. 1525.
[41] W. Shang, F. Wu, Y.Q. Wen, C.B. He, X.Q. Zhan, and Y.Q. Li, Corrosion resistance and mechanism of graphene oxide composite coatings on magnesium alloy, *Ind. Eng. Chem. Res.*, 58(2019), No. 3, p. 1200.
[42] C.Q. Wu, Q. Liu, R.R. Chen, *et al.*, Fabrication of ZIF-8@SiO_2 micro/nano hierarchical superhydrophobic surface on AZ31 magnesium alloy with impressive corrosion resistance and abrasion resistance, *ACS Appl. Mater. Interfaces*, 9(2017), No. 12, p. 11106.
[43] A. Fattah-Alhosseini, R. Chaharmahali, and K. Babaei, Effect of particles addition to solution of plasma electrolytic oxidation (PEO) on the properties of PEO coatings formed on magnesium and its alloys: A review, *J. Magnes. Alloys*, 8(2020), No. 3, p. 799.
[44] A. Bordbar-Khiabani, B. Yarmand, and M. Mozafari, Enhanced corrosion resistance and *in-vitro* biodegradation of plasma electrolytic oxidation coatings prepared on AZ91 Mg alloy using ZnO nanoparticles-incorporated electrolyte, *Surf. Coat. Technol.*, 360(2019), p. 153.
[45] H.P. Duan, C.W. Yan, and F.H. Wang, Growth process of plasma electrolytic oxidation films formed on magnesium alloy AZ91D in silicate solution, *Electrochim. Acta*, 52(2007), No. 15, p. 5002.
[46] Z.R. Zheng, M.C. Zhao, L.L. Tan, *et al.*, Corrosion behavior of a self-sealing coating containing CeO_2 particles on pure Mg produced by micro-arc oxidation, *Surf. Coat. Technol.*, 386(2020), art. No. 125456.